Z. Lin and W. Han

DOI: 10.1002/anie.201104454

Self-Assembly

Learning from "Coffee Rings": Ordered Structures Enabled by Controlled Evaporative Self-Assembly

*Wei Han and Zhiqun Lin**

Keywords:
coffee rings · confined geometry · controlled evaporative self-assembly · hierarchically ordered structures

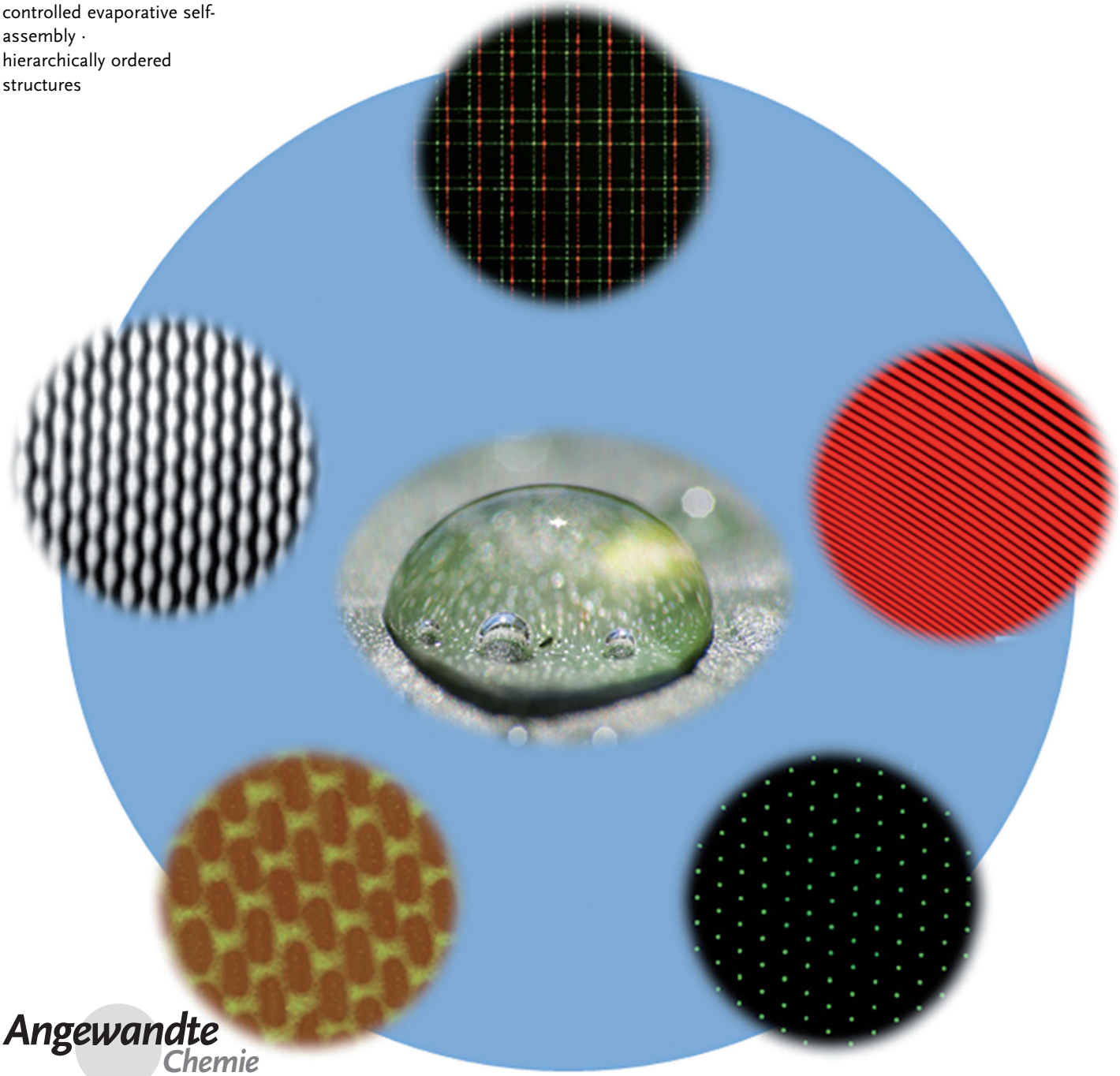

Research into the evaporation of solutions is not only aimed at a better understanding the physics of evaporation, but increasingly at capitalizing on the extremely simple method it offers to assemble diverse nonvolatile solutes into complex ordered structures on the submicron and longer length scales. This Review highlights recent advances in evaporative assembly of confined solutions, focusing especially on recently developed approaches that provide structures with unprecedented regularity composed of polymers, nanoparticles, and biomaterials, by controlled evaporation-driven, flow-aided self-assembly. A broad range of variables that can control the deposition are explored and the future directions of this rich field are presented.

From the Contents

1. Introduction

Drying a drop of solution containing nonvolatile solutes (e.g., polymers, proteins, viruses, bacteria, DNA, microspheres, nanoparticles, graphenes) on a solid surface has been widely recognized as a simple, emergent technique to yield self-assembled, dissipative 1D or 2D structures with controlled dimensions (a few hundred submicrons and more), function, and topology.[1] These structures are kinetically trapped in non-equilibrium states, meaning that they depend sensitively on the evaporative route taken. Experimentally, the types of deposit are correlated with the mode of liquid evaporation. The most familiar deposits are the "coffee ring" patterns. When a spilled drop of coffee dries on a solid surface, it leaves a dense, ring-like deposit along the perimeter, i.e., forming "coffee ring" on the surface. Ringlike stains are not particular to coffee and are commonly seen in the drops containing dispersed solutes.[1a] In the absence of natural convection and Marangoni flow driven by surface tension gradient, when the contact line of a drying droplet is pinned, the liquid evaporating from the edge is replenished by the liquid from the interior, so the outward flow carries entrained solutes to the drop periphery (upper panel in Figure 1 a), yielding a dense, ringlike deposit (lower panel in Figure 1 a). Notably, the deposition-caused pinning and depinning processes (i.e., "stick–slip" motion) alternate as solvent evaporates, thereby forming concentric rings after complete evaporation of the solution.[2] However, the concentric rings are often stochastically distributed. Conversely, if the liquid inside the droplet flows away from the contact line, a uniform solute deposit on the substrate may result.[3] It is noteworthy that, based on the continuity and Navier–Stokes equations within a lubrication approximation, the majority of current theoretical studies have focused on modeling a single "coffee-ring" deposit using either analytical[1b,4] or numerical methods.[3,5] In contrast, only a few elegant theoretical studies have centered, either analytically[2a] or numerically,[6] on elucidating the formation of periodic concentric rings for a sessile droplet drying on a substrate. The surface-tension driven convective instability of a drying droplet heated from below and cooled from above is referred to as the Marangoni–Benard convection (top and center panels in Figure 1 b), which leads to the formation of irregular cellular structures (i.e., Benard cells; bottom panel in Figure 1 b).[7] The fingering instability of thin spreading films is caused by the Marangoni effect, in which a temperature gradient induces a surface-tension gradient that drives the spreading process at the liquid front (Figure 1 c).[9] Additionally, a fingering instability can also be induced by unfavorable interfacial interactions between the solute and the substrate.[10] However, primarily because of the spatially varied evaporative flux and possible convections, these dissipative structures (e.g., "coffee rings",[1a] polygonal network structures,[7c] fingering instabilities,[11] cracks, chevron patterns, etc.) are generally irregular and randomly assembled. Yet for many applications in optics, microelectronics, optoelectronics, magnetic devices, biotechnology, and nanotechnology, it is highly desirable to achieve surface patterns with well-controlled spatial arrangements.

Clearly, to exploit the full potentials of this nonlithographic and external-field-free technique to construct highly ordered, complex structures rapidly and cheaply over large areas, the evaporation process and associated flow velocity field should be precisely harnessed. Recently, a few impressive studies have demonstrated the feasibility of delicately manipulating the drying process to drive the assembly of inorganic nanoparticles, polymers, and biological entities into intriguing, well-structured patterns. These drying techniques include controlled anisotropic wetting/dewetting processes,[12] controlled dewetting by dip-coating,[13] convective assembly in evaporating menisci,[14] evaporation-induced assembly in restricted geometries,[15] and evaporative lithography using a mask.[16]

In this Review, we aim to highlight the current state-of-the-art in controlled evaporative self-assembly (CESA) of constrained solutions, a process that enables the organization of materials of interest (polymers, nanoparticles, and biomaterials, among others) into complex structures of high fidelity and regularity with engineered optical, electronic, optoelectronic, magnetic properties. Five facile yet robust preparation approaches that yield highly ordered structures based on

[*] W. Han, Prof. Z. Lin
School of Materials Science and Engineering, Georgia Institute of Technology
771 Ferst Drive, NW, Atlanta, GA 30332-0245 (USA)
E-mail: zhiqun.lin@mse.gatech.edu

CESA of droplets in confined geometries are highlighted. The drying of unconstrained solutions that leads to ordered structures is not discussed herein. For details on this subject the reader is referred to some relevant Reviews.[17] We suggest a large number of important variables that can be tailored to control deposition. Finally, we indicate the significance of these approaches and offer a perspective for future work that is certainly exciting yet scientifically and technologically challenging in this extraordinarily rich field.

2. Controlled Evaporative Self-Assembly (CESA) in Confined Geometries

In stark contrast to structures formed from a freely evaporating droplet on a substrate (that is, unconstrained solution), which are often stochastic and lack regularity, the judicious use of confined geometries (e.g., two parallel plates, "curve-on-flat" geometries) imparts exquisite control over the drying dynamics and associated flows, which in turn, allows for crafting complex deposit patterns with unprecedented regularity. By subjecting drying droplets to such a restricted geometry, the evaporation rate of the solution is controlled and the temperature gradient is minimized or eliminated. As a result, the possible natural convection and Marangoni flow are suppressed, and the instabilities (e.g., fingering instability) can be readily controlled.

2.1. Geometry Utilized

The rational design and implementation of confined geometry offers the opportunity for achieving well-structured assemblies, and thereby providing a new assembly route to create complex yet ordered functional micro- to nanoscale structures that can potentially be used in various technological applications. To date, five viable geometries have been designed and successfully exploited for the CESA of constrained solutions. These are a) two-plate configuration in which the upper plate is positioned either at a certain angle against[14,18] or parallel to[15a,b] the lower horizontal plate and one plate slides over the other at a fixed angle and distance (Figure 2 and Figure 3); b) cylindrical tubes (Figure 5);[15j,k,19] c) two crossed cylinders placed at right angle (Figure 7);[15c] d) mask-above-drying-film configuration (i.e., evaporative lithographic patterning[16a,20]; Figure 8); and e) "curve-on-flat" geometries (Figure 9–12).[10,15d–i,21]

2.2. Flow-Based Processing in Two-Plate Geometry

Self-assembly of nanoscale materials into desired structures with spatially defined structure and functionality promises new opportunities for their use in miniaturized electronics, photonics, catalysts, nanotechnology, and biotechnology. Recently, controlled patterns of quantum dots (QDs) stripes have been produced by a simple flow-coating technique, in which the motion of the lower plate was regulated while the upper blade, placed at a certain angle, was stationary, thereby providing a confined geometry for QD deposition (Figure 2a).[18b] QDs are highly emissive, spherical, inorganic nanoparticles a few nanometers in diameter. They offer a functional platform for a new class of materials for use in light emitting diodes (LEDs), photovoltaic cells, and biosensors.[22] For QDs, such as CdSe, the variation of particle size provides continuous and predictable changes in fluorescence emission as a result of their quantum-confined nature.[23] The combination of confined geometry and controlled nanoparticle deposition which is enabled by programming the rate and direction of lower plate on the linear translational stage, provided distinct advantages in the assembly of nanomaterials (Figure 2b), yielding both parallel and orthogonal multicomponent CdSe stripe patterns with controllable spacing between them. For example, green-emitting vinylbenzene-functionalized CdSe QDs (diameter, $D = 3$ nm) were first assembled into stripes by flow coating (vertical green stripes in Figure 2c), which were then subjected to UV irradiation to crosslink the vinylbenzene ligands of the CdSe QDs. The second (i.e., vertical red-emitting QD stripes, $D = 6$ nm) and third (i.e., horizontal green-emitting QD stripes) stripe patterns were then deposited parallel and perpendicular to the first green stripes, respectively (Figure 2c).[18b] The QD stripes were nanometers high, submicron to micron wide and centimeters long. In addition to CdSe QDs, the flow-coating technique allows the structuring of materials of different types and sizes (e.g., Au

Wei Han is a Ph.D. student in the Department of Materials Science and Engineering at Iowa State University. He studied Physics at Nanjing University, China (B.S. 2006, and M.S. 2009). He has been a research assistant in Professor Zhiqun Lin's nanostructured functional materials (NanoFM) group since 2009. His research interests include preparation of highly ordered complex structures of various materials (polymers, nanoparticles and biomaterials), by controlled evaporative self-assembly (CESA), hierarchical structure formation, magnetic-field-induced self-assembly, and surface wrinkling.

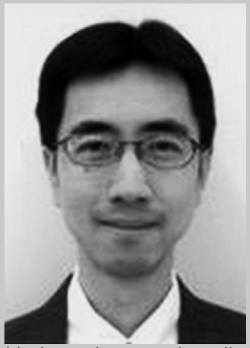

Zhiqun Lin received the Master degree in Macromolecular Science from Fudan University, Shanghai in 1998 and the PhD degree in Polymer Science and Engineering from UMass, Amherst in 2002. He was a postdoctoral associate at UIUC. He joined the Department of Materials Science and Engineering at Iowa State University in 2004 and was promoted to Associate Professor in 2010. He moved to Georgia Institute of Technology in 2011. His research interests include hierarchical structure formation and assembly, surface and interfacial properties, block copolymers, solar cells, conjugated polymers, and multifunctional nanocrystals. He is a recipient of an NSF Career Award and a 3M Nontenured Faculty Award.

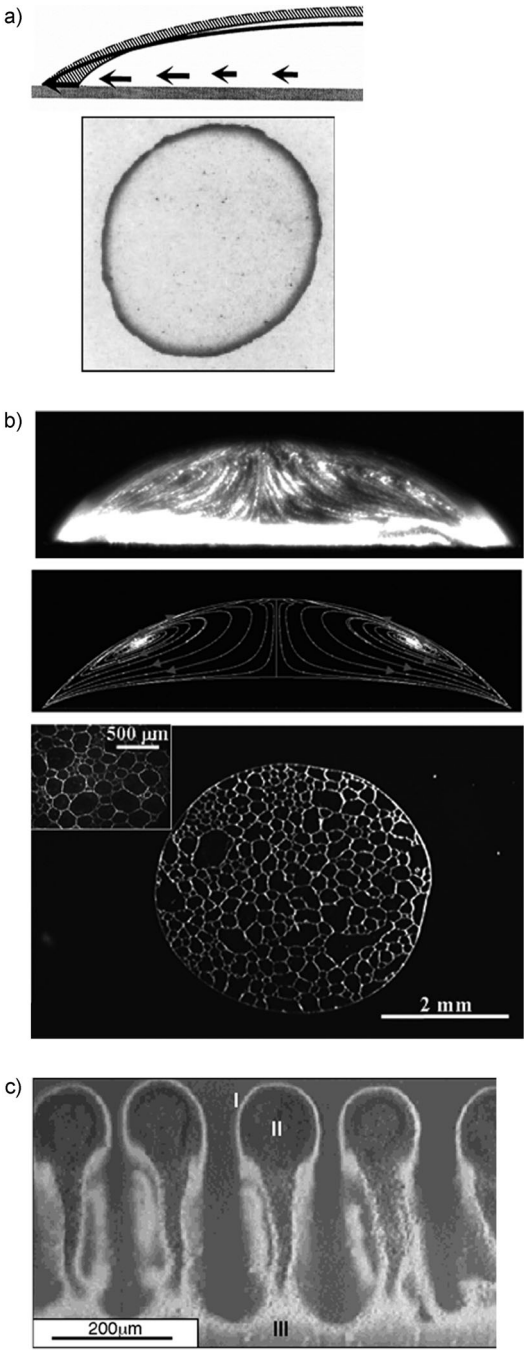

Figure 1. Characteristic patterns yielded from evaporative assembly of drying droplets. a) "Coffee ring" deposits. Top: the mechanism of outward flow during evaporation to keep the contact line fixed. Reproduced with permission from Ref. [1a]. Bottom: a "coffee ring" with a radius of approximately 5 cm. Reproduced with permission from Ref. [8] b) Top: Marangoni vortex flow field in a drying octane droplet. Middle: the simulation result. Reproduced with permission from Ref. [7f]. Bottom: cellular structure of microspheres. Reproduced with permission from Ref. [8c]. c) The fingering instability at the liquid front. Reproduced with permission from Ref. [9].

nanoparticles, PMMA, and PDMS) at different spatial locations.[18b]

Similarly, controlled deposition of latex colloidal crystal suspensions and Au nanoparticles confined in a meniscus was

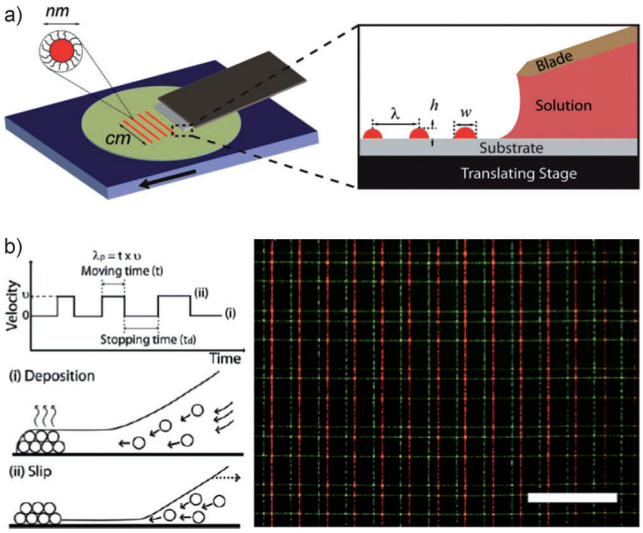

Figure 2. a) Schematic diagram of two-plate configuration in which a QD solution is confined. The upper plate (blade) is placed at a certain angle over the lower movable substrate on a translation stage (i.e., a flow-coating apparatus). b) The velocity profile of a translation stage for controlling the "stick–slip" motion of the contact line. Schematic illustrations of QD deposited i) at intermittent stopping time and ii) upon the move the translating stage. c) A fluorescent micrograph of grid patterns formed by a three-step flow-coating process. Scale bar = 200 μm. Reproduced with permission from Ref. [18b].

performed by dragging the upper blade (i.e., deposition plate) at a constant velocity, while fixing the lower plate, forming a thin particle film.[14,18a] The number of particle layers and structures were determined by the deposition speed and the particle volume fraction.[14] In comparison to conventional dip-coating, this convective assembly approach offered reduced material consumption and shorter coating time.[14]

When a polymer solution was placed between two precisely manipulated parallel plates with a stationary lower substrate and a sliding upper surface, a variety of polymer patterns were produced at the receding meniscus on the lower substrate (Figure 3).[15a] Three mechanisms, namely, dewetting, "stick–slip" motion, and fingering instabilities, were proposed to account for the formation of dots, lines, and ladder-like structures, respectively (Figure 4). The concentration of polymer solution governed the self-organization of mesoscale polymer patterns from the evaporating solution edge.[15a] Moreover, faster sliding of the upper surface increased the surface area of the meniscus region where the evaporation occurred, thus resulting in an increase in deposition frequency, and correspondingly, a decrease in the spacing of patterns.[15a] In addition to polystyrene (PS) and poly(3-hexylthiophene) (P3HT) utilized in the study, this preparation method is applicable to pattern other polymer materials. Recently, hierarchical assembly has been achieved using a lamellar-forming diblock copolymer, polystyrene-*b*-poly(methyl methacrylate) (PS-*b*-PMMA; $M_{n,PS} = 52\ kg\,mol^{-1}$ and $M_{n,PMMA} = 52\ kg\,mol^{-1}$) as nonvolatile solutes.[15b,24] The microstripes were formed from the receding contact line of PS-*b*-PMMA solution confined in a two-parallel-plate geometry. Subsequent thermal annealing at

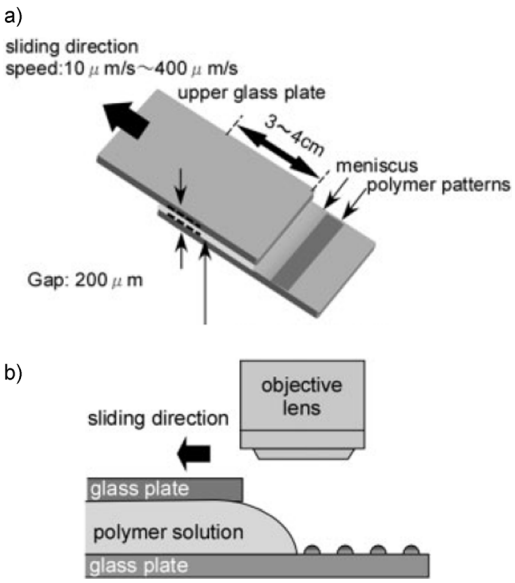

Figure 3. Schematic illustrations of the two-parallel-plate geometry in which the upper plate slides over the lower stationary plate at a fixed speed. a) 3D view and b) side view, where a polymer solution is confined between the two parallel plates. Reproduced with permission from Ref. [15a].

high temperature led to the alignment of lamellae along the thickness gradient of the patterned film.

2.3. Producing Bands of Particles in Cylindrical Tube

The ability to pattern curved surfaces that are topologically complex (e.g., in a capillary tube) opens new avenue for making microfluidic devices for sensing and catalysis, as well as for utilizing colloidal-coated capillaries to probe the influence of varied film thickness on optical properties.[15j] The confinement imposed by a capillary tube created a fluidic column, from which bands of particle aggregates were produced along the tube, either vertically (Figure 5a)[15j] or horizontally (Figure 5b and 6)[15k]. Recently, colloidal crystallization and banding in a vertically arranged 400 μm diameter cylindrical tubes were studied.[15j] The contact line of PS beads ($D = 500$ nm) in an ethanol solution was pinned by the deposition of particles. The length of deposits increased until the capillary force can no longer counterbalance the gravitational force, after which the contact line dropped to a new position where the solution was in contact with the tube surface.[15j] The capillary force was determined by the radius of curvature of the tube which was much smaller than the capillary length. The distance traveled by the contact line was given by $\Delta h = h^{SG} - h^{SP} = (\gamma/\rho g a)(\cos\theta_{SG} - \cos\theta_{SP}) \approx 1$ mm, which was in good agreement with the experimental observation, where γ is the surface tension of ethanol, $\gamma \approx 20\ \mathrm{mN\,m^{-1}}$, $\theta_{SG} = 5°$ and $\theta_{SP} = 60°$ are solvent/glass contact angle and solvent/PS contact angle, respectively.[15j] As the meniscus fell, the evaporation rate in the capillary tube decreased. In other words, the vapor diffusion length increased as the distance to the open end of the capillary increased, which in turn led to the deposition of fewer PS particles, thereby yielding narrower bands of PS as the time progressed (i.e., forming gradient bands). Importantly, the use of a capillary tube effectively regulated the evaporation rate of the fluidic column, which in turn influenced the kinetics of colloidal crystallization giving a banded structure (Figure 5c). The band width and the spacing between the neighboring bands (i.e., the distance traveled by the contact line) increased with an increase of colloidal concentration or

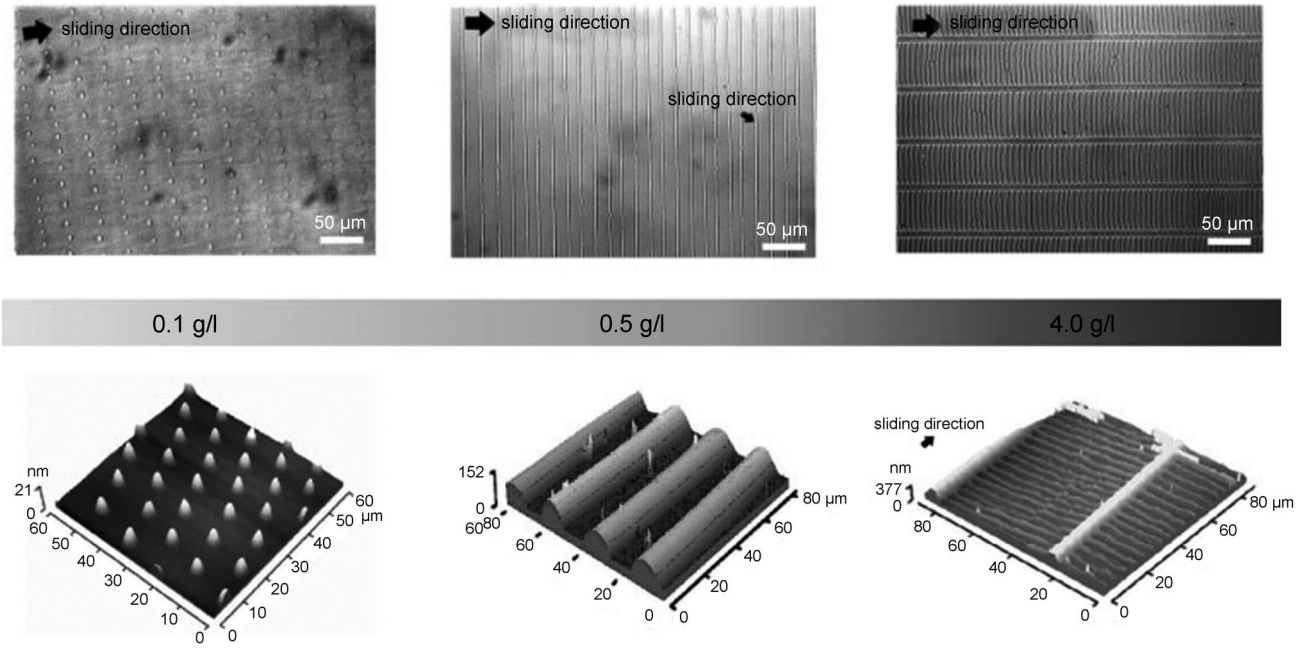

Figure 4. Optical micrographs (top panels) and AFM images (bottom panels) of PS patterns produced from different solution concentrations at a constant sliding speed of 50 μm s^{-1}. Reproduced with permission from Ref. [15a].

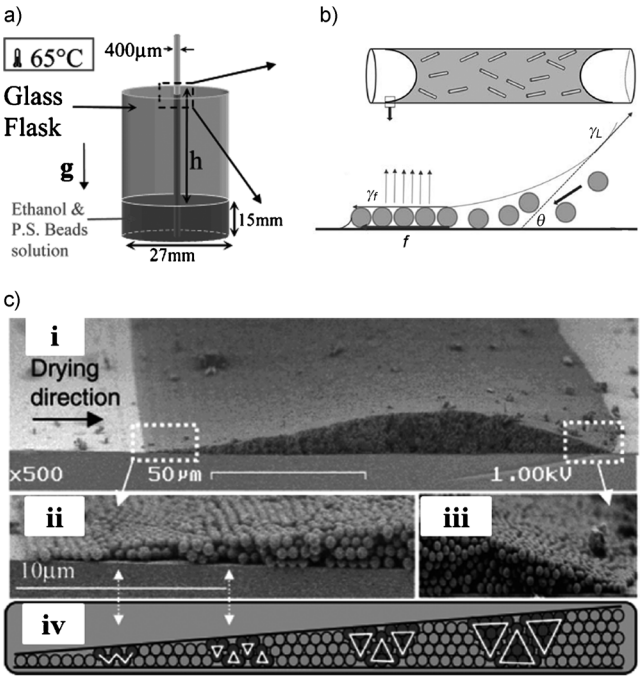

Figure 5. Schematic illustrations of a cylindrical capillary placed a) vertically and b) horizontally, that yields bands of particle aggregates (i.e., PS particles in (a) and tobacco mosaic virus (TMV) particles in (b)). In (b), Top: a capillary tube containing the TMV solution; Bottom: a thin meniscus formed at the contact line. Reproduced with permission from Ref. [15k]. c) SEM images of a band structure in the capillary. i) One band with the drying direction indicated. Two close-ups of smooth structure at the beginning (ii) and the end (iii) of the band, respectively. iv) Schematic illustration of a typical succession of hexagonal close-packed regions. Reproduced with permission from Ref. [15j].

with a decrease in time at a given initial concentration of PS solution.[15j]

Likewise, banded structures composed of rodlike bionanoparticles (tobacco mosaic virus (TMV)) have been produced by CESA in a horizontally placed glass capillary tube (length, $L = 2.2$ cm and $D = 0.15$ cm; Figure 6).[15k] At the fixed salt concentration, bands made of a monolayer of TMV particles were formed at low TMV concentration (Figure 6), while multilayers of TMV in each band were yielded as the TMV concentration increased. Further increase in concentration led to a disappearance of bands, and the tube was fully covered with TMV particles. At very high concentration, zigzag patterns resulted. It is worth noting that the TMV particles were oriented parallel to the contact line (i.e., perpendicular to the long axis of the tube). In addition to concentration, the salt and surface properties of the capillary-tube interior exerted a significant effect on the pattern formation. For example, in the absence of salt, at high TMV concentration, a continuous TMV thin film was produced with TMV aligned normal to the contact line (i.e., along the long axis of the tube) as a result of strong dipole–dipole repulsion between TMV nanorods. The TMV-patterned capillary tube can be utilized as a template to direct the orientation of smooth muscle cells (SMCs) cultured in the tube for developing enhanced vascular grafts.[15k]

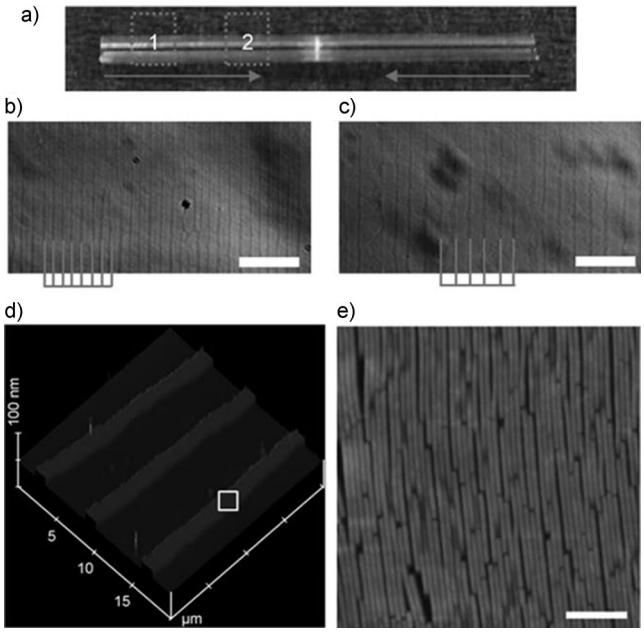

Figure 6. Self-assembly of rod-like TMV nanoparticles in a glass capillary tube. a) Glass capillary tube. b) and c) Optical micrographs of stripe patterns formed at position 1 and position 2 marked in (a), respectively. d) 3D AFM image of stripe patterns shown in (b). e) A close-up of the white-boxed region labeled in (d). Scale bar = 50 μm in (b) and (c); and scale bar = 200 nm in (e). Reproduced with permission from Ref. [15k].

2.4. Assembling in Two-Crossed Cylinders

Recently, the use of a restricted geometry comprising two cylindrical quartz mounts placed at right angles to one another, glued with freshly cleaved single crystals of mica, constrained the evaporation occurring at the droplet edges (Figure 7) and organized surface patterns of remarkably high

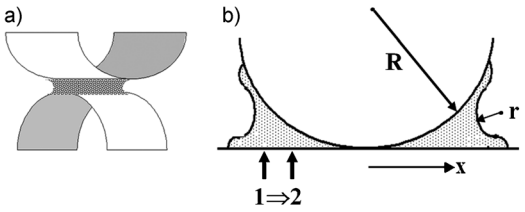

Figure 7. a) Schematic illustrations of two crossed cylinders of freshly cleaved single crystals of mica. b) The crossed cylinders are brought together, leading to the formation of a constrained solution with an evaporation rate that is highest at the extremity. Reproduced with permission from Ref. [15c].

fidelity and regularity.[15c] The nonvolatile component was a drop of linear conjugated polymer, poly[2-methoxy-5-(2-ethylhexyloxy)-1,4-phenylenevinylene] (MEH-PPV; $M_W = 50$–$300\ kg\,mol^{-1}$), in toluene solution. Conjugated polymers have been widely recognized as promising materials for use in biosensors, thin film transistors, light-emitting diodes, and solar energy conversion.[23a,f,25] In the latter context, conjugated polymer-based photovoltaic devices capitalize on the

advantages peculiar to conjugated polymers, such as light weight, flexibility, processability, roll-to-roll production, low cost, and large area.[26] The repetitive pinning–depinning of the contact line, which moved toward the mica/mica contact center as time elapsed, producing hundreds of concentric MEH-PPV rings over large areas.[15c] Each ring was approximately nanometers high and micrometers wide. The spacing between adjacent rings, λ, and the height of ring, h decreased as a function of the distance from the mica/mica contact center (i.e., $\lambda \approx (\Delta x)^{0.009}$ and $h \approx (\Delta x)^{0.017}$, where Δx denotes the change in distance). The observed micrometer-size rings were governed by the imposed geometry, the solution concentration, and the solvent properties.[15c]

2.5. Patterning Colloid Films by Evaporative Lithography

It is interesting to note that a novel approach termed evaporative lithography has recently emerged as a simple route to assemble unary (e.g., silica microsphere, $R = 0.59$ μm) and binary (e.g., silica microsphere, $R = 0.59$ μm and PS nanoparticles, $R = 10$ nm) colloidal films without substrate modification.[16,20] A drying colloidal suspension was allowed to evaporate beneath a mask containing a hexagonal array of micro-sized holes, which induced periodic variations between regions of hindered and free evaporation (Figure 8a).[16,20] When silica microspheres were used, at the low volume fraction, $\phi_{SiO_2} = 0.005$, discrete patterned features formed ((i) in Figure 8c). As ϕ_{SiO_2} exceeded a critical initial volume fraction, $\phi^*_{SiO_2}$, a transition from hexagonally arranged patterns to continuous patterned films occurred ((ii) in Figure 8c). At high ϕ_{SiO_2} (i.e., $\phi_{SiO_2} > \phi^*_{SiO_2}$), thicker films with patterned surface were formed ((iii) in Figure 8c).[16a] The finite-element modeling (FEM) analysis revealed that the maximum evaporative flux, J_{max} was reached under the unmasked regions of the drying film (i.e., open regions), while the minimum evaporative flux, J_{min} occurred under the masked regions.[16a] As a result, the microspheres migrated toward the unmasked regions and were arrested there, forming patterned deposits. The deposition profiles can also be controlled by tuning the separation distance between the mask and underlying film and mask design.[16a] Clearly, either small h_g (the initial gap height between the mask and underlying film; Figure 8b) or large P (the pitch; Figure 8a) hindered evaporation under the masked regions. The suppression of evaporation diminished as h_g was increased or P was decreased.

Quite intriguingly, the evaporative lithography technique was capable of directing the distribution of multicomponent systems simultaneously during drying. By drying a film of binary suspension (0.59 μm silica microsphere and 10 nm PS nanoparticles, $\phi_{SiO_2} = 0.3$ and $\phi_{PS} = 0.001$) under the mask, the silica microspheres formed a continuous patterned film, whereas the PS nanoparticles segregated to the open regions, decorating the surface of the microspheres.[16a] At the early stage of the drying process, the silica microspheres and PS nanoparticles were transported to the open regions by particle convection. The higher initial volume fraction of microspheres ($\phi_{SiO_2} = 0.3$) made them rapidly coalesce into a closely packed network with many interstitial pores. The nanoparticles ($\phi_{PS} = 0.001$) were then transported through the porous microsphere network and further driven by a pressure gradient resulting from the receding liquid meniscus, to segregate in the unmasked regions of the binary film.[16a] The evaporative lithography opens up a promising new avenue for organizing a wide range of soft materials, including polymers, biomolecules, and colloids.[16a]

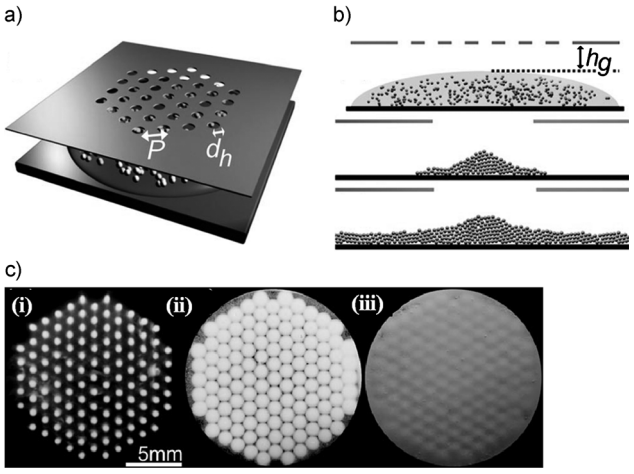

Figure 8. Schematic illustration of evaporative lithography. a) Top view and b) side view of the mask design, where P is the pitch and d_h is the hole diameter. b) Top: a discrete pattern prepared from a dilute suspension; Middle and Bottom: a continuous patterned film produced from a concentrated suspension. c) Optical micrographs of films from the drying of colloidal suspensions at i) $\phi_{SiO_2} = 0.005$, ii) $\phi_{SiO_2} = 0.1$, and iii) $\phi_{SiO_2} = 0.3$. Reproduced with permission from Ref. [16a].

2.6. Controlled Evaporative Assembly (CESA) in "Curve-on-Flat" Geometry

If a drop of solution to evaporate is constrained in a "curve-on-flat" geometry composed of a curved upper surface situated on a flat substrate (i.e., forming a capillary-held solution), a multitude of strikingly regular structures can be created.[10,15d–i,21a–i] The rationally designed "curve-on-flat" geometry provides a unique environment for remarkable control over the flow within the evaporating droplet, and thus regulating intriguing structure formations. The conceptually simplest configuration is the "sphere-on-flat" geometry which is constructed by placing an axially symmetric spherical lens (e.g., a silica sphere) on a flat substrate (e.g., silicon, ITO glass, or mica). Recently, highly regular concentric rings of MEH-PPV were formed spontaneously, simply by allowing a drop of MEH-PPV toluene solution to dry in a consecutive "stick–slip" motion in the "sphere-on-Si" geometry (Figure 9).[15f] Because of the imposed geometrical restriction, the evaporation could only occur at the capillary edge where, at its extremity, the evaporation rate was highest. As the toluene evaporated, the contact line at the capillary edge was pinned by transporting MEH-PPV from the center of the solution ("stick"), thus forming the outermost "coffee ring" of MEH-

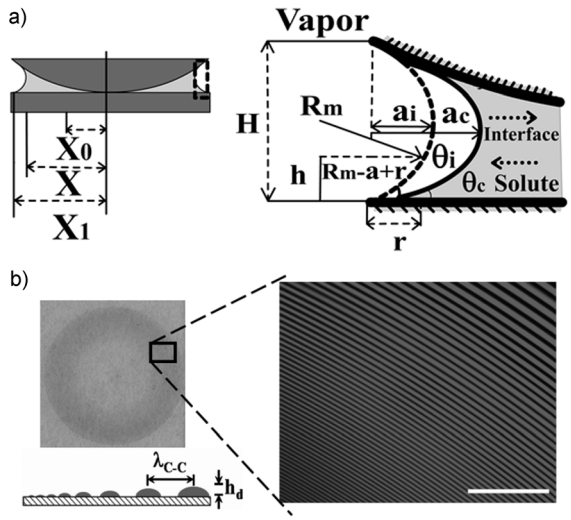

Figure 9. a) Left: Schematic cross section of a capillary-held solution containing a nonvolatile solute placed in a "sphere-on-flat" geometry. X_1, X, and X_0 are the radii of outermost, intermediate, and innermost rings from the sphere/flat contact center, respectively. Right: close-up of the capillary edge marked in the left panel. b) Left: Digital image of entire gradient concentric rings formed by the deposition of MEH-PPV in the geometry shown in (a). Right: A small zone of the fluorescent image of MEH-PPV rings in red is shown. Scale bar = 200 μm. As the solution front moves inward, the rings become smaller and the height decreases as illustrated in lower left schematic. Reproduced with permission from Ref. [15f].

PPV. During this process, the initial contact angle of the meniscus, θ_i gradually decreased owing to the evaporative loss of toluene, to a critical angle, θ_C (Figure 9a), at which the capillary force (the depinning force) became larger than the pinning force. This change led the contact line to jerk toward the sphere/Si contact center ("slip") and be arrested at a new position, and thus a new "coffee ring" of MEH-PPV was deposited.[15f] The repeated pinning and depinning cycles of the contact line produced gradient concentric rings with controlled spacing as a direct consequence of the competition between the linear pinning force ($F_{pin} \approx 2\pi X$, where X is the absolute position of the ring from the sphere/Si contact center (Figure 9a)) and nonlinear capillary force ($F_c = 16\pi\gamma_{lv} X \arctan(4aR/X^2)$, where γ_{lv} is the surface tension of solvent, and a and R are the height of meniscus and the radius of curvature of sphere, respectively) because of the curvature effect of upper spherical lens.[15f] As clearly shown in Figure 9b, the center-to-center distance between adjacent rings, $\lambda_{C\text{-}C}$, and the height of ring, h_d decreased with increasing proximity to the sphere/Si contact center. Theoretical calculations based on the mass conservation of confined solution and the Navier–Stokes equation within a lubrication approximation after considering the evaporation process were successfully performed to gain insight into the formation of gradient patterns in $\lambda_{C\text{-}C}$ and h_d, respectively, which agreed well with experimental observations.[15f] In addition to concentric rings of polymers, nanoparticles,[15g,21h] carbon nanotubes,[21d] graphenes,[27] other ordered yet complicated structures were also produced in the "sphere-on-flat" geometry, including spokes,[15g] fingers,[10,21c] "snake-skin",[21g] serpentines,[15i] by carefully manipulating the size of nanocrystals used[15g] and the interfacial interaction between the solute and substrate.[10,15i,21c]

Instead of using a spherical lens, by logically designing the upper surface to accommodate different shapes (i.e., crafting a "curve-on-flat" geometry), "coffee rings" of different forms and sizes can be specifically "synthesized". A simple route to concentric square stripes has been recently demonstrated by confining the MEH-PPV toluene solution in the "square-pyramid-on-flat" geometry (Figure 10a,b). The pyramid (i.e., the upper surface) directed the "stick–slip" motions of the drying MEH-PPV microfluid, thereby guiding MEH-PPV to deposit in a manner that conformed to the square-shaped sides of the pyramid (Figure 10b and c). Consequently, repeated "stick–slip" cycles of the contact line resulted in the formation of hundreds of concentric squares of MEH-PPV (Figure 10c).[15h] A 90° bending of concentric squares on the border (corner) formed by two facets of the square pyramid is clearly evident (upper left panel, Figure 10c), while parallel stripes were observed under the facets of the pyramid (upper right panel, Figure 10c). A transition from

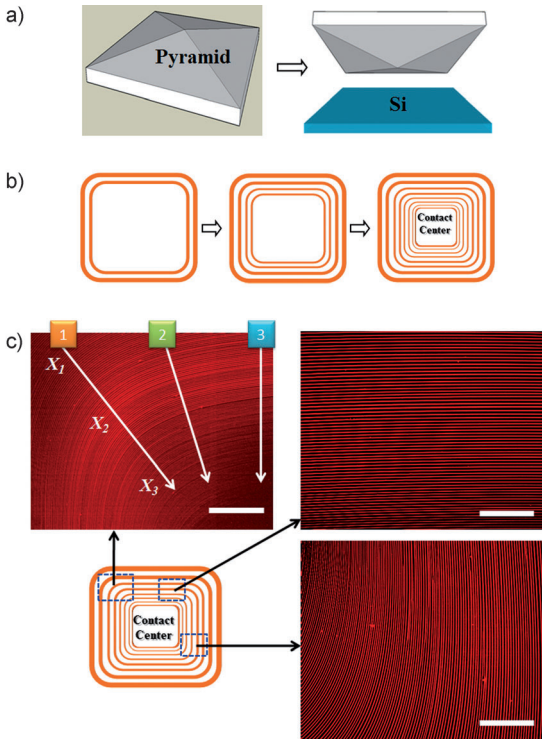

Figure 10. a) Schematic illustration of the construction of a "square-pyramid-on-Si" geometry. b) Stepwise representation of the formation of gradient concentric square stripes, propagating from the capillary edge towards the pyramid/Si contact center during solvent evaporation. c) Representative fluorescence micrographs corresponding to locations defined in the bottom left schematic (dashed blue boxes) showing the bent stripes (top left and bottom right micrographs) and parallel straight stripes of MEH-PPV (top right micrographs) formed on the Si substrate. Scale bars are 600 μm in the top left and 300 μm in the top and bottom right images. Reproduced with permission from Ref. [15h].

bent to parallel stripes is shown in the lower right panel of Figure 10c.[15h] By replacing the square pyramid with a triangular-slice sphere as the upper surface, a set of concentric triangular contour lines of MEH-PPV can be readily produced as shown in representative fluorescence micrographs (Figure 11c). The construction of a "triangular-slice-sphere-on-flat" geometry is illustrated in Figure 11a. The ability to guide a variety of intricate structural formations by CESA allows for the scale-up of surface patterning over large areas at low cost, and displaces the need for lithography and external fields.[15h]

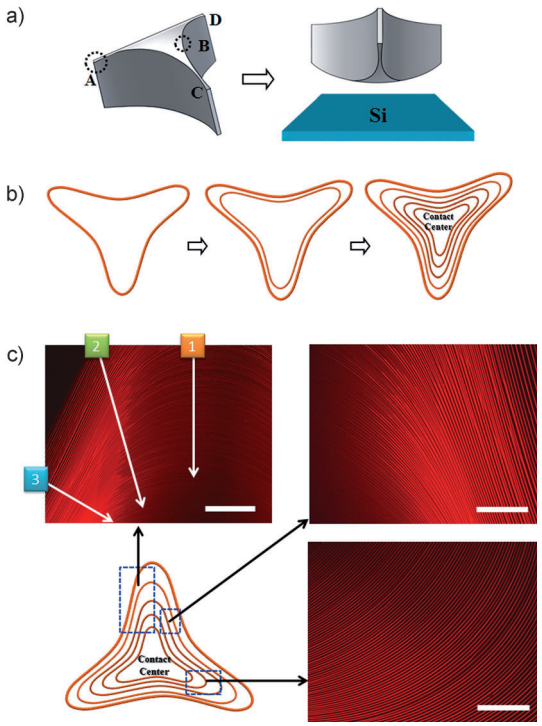

Figure 11. a) Schematic illustration of the construction of "triangular-slice-sphere-on-Si" geometry. b) Stepwise representation of the formation of gradient concentric triangular contour lines in the "triangular-slice-sphere-on-Si" geometry. c) Representative fluorescence micrographs at different locations defined in the bottom left schematic (dashed blue boxes) showing the highly curved lines. Scale bars are 600 μm in the top left and 300 μm in the top and bottom right images. Reproduced with permission from Ref. [15h].

Controlling the spatial arrangement of components, namely, forming hierarchically ordered structures, has attracted considerable attention as they hold great promise for numerous applications. To date, many studies have centered on creating hierarchically ordered structures using destructive lithographic techniques that involve maintenance costs and require iterative, multi-step procedures, thereby making the structure formation process more complex and less reliable.[15e] In contrast, the ability to engineer hierarchically organized structures from the self-assembly of nanomaterials, that is, generating microscopic structures from materials with a self-assembling nature at the nanometer scale, dispenses with the need for lithography and external fields and opens new opportunities for the materials to be used in optical, electronic, optoelectronic, and magnetic materials and devices.[15e] Recently, a simple yet robust method to create hierarchically ordered structures consisting of diblock copolymers using two consecutive self-assembly processes at different length scales was demonstrated.[15e,i,21i] Diblock copolymers composed of two chemically distinct chains covalently linked at one end are thermodynamically driven to self-assemble into a broad range of well-ordered nanodomains (e.g., spheres, cylinders, and lamellae) depending on the volume fraction of the components.[28] The domain size is governed by the molecular weight and is typically on the scale of 10 to 100 nm, which gives a density of 10^{13} nanostructures per square inch (1 inch = 2.5 cm). As such, diblock copolymers are widely recognized as appealing building blocks for the bottom-up nanofabrication for numerous applications, such as photonic devices, nanoelectronics, magnetic data storage, biosensor arrays, and nanotechnology.

The CESA of a diblock copolymer solution, for example, a toluene solution of cylinder-forming PS-*b*-PMMA (PS block forming nanocylinders in the PMMA matrix), together with controlled fingering instabilities arising from unfavorable interfacial interactions between the PS block and the Si substrate in the "sphere-on-Si" geometry, yielded large concentric serpentines of PS-*b*-PMMA at the microscopic scale (first panel in Figure 12a and top left panel in Figure 12b). Subsequently, upon selective solvent-vapor annealing (that is the selective swelling of the PMMA block by acetone vapor), the serpentines self-organized into a macroscopic web (last panel in Figure 12a and top right panel in Figure 12b), and simultaneously, the PS block self-assembled into nanocylinders that were oriented vertically to the web

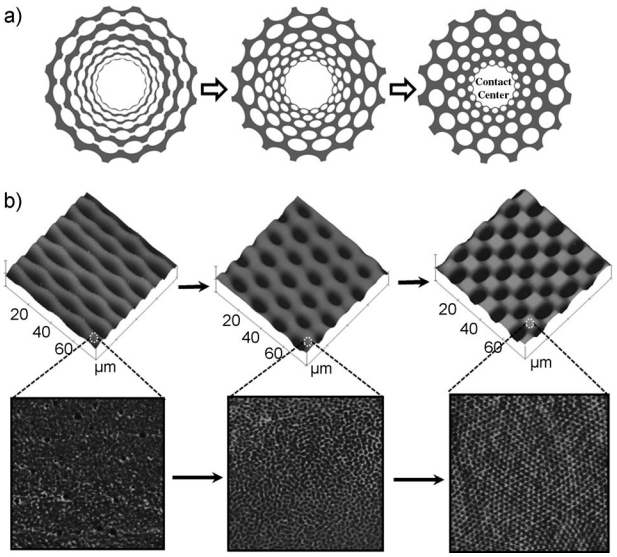

Figure 12. a) Schematic illustration of spatial–temporal evolution of concentric PS-*b*-PMMA serpentines into web-like macrostructures after lengthy solvent-vapor annealing. b) Evolution of regular PS-*b*-PMMA serpentines into hierarchically woven mesh arrays by acetone-vapor annealing. Top: AFM height images; scan size = 80×80 μm^2. Bottom: AFM phase images; scan size = 2×2 μm^2. The originally featureless surface topology (bottom left) transforms into well-ordered PS nanocylinders (bottom right). Reproduced with permission from Ref. [15i].

surface (bottom right panel in Figure 12b). The resulting remarkably ordered structures exhibited two distinctive dimensions: global web-like macrostructures with local regular microporous mesh arrays by a top-down mechanism; and, by a bottom-up approach, vertically oriented PS nanodomains that spanned the entire web (i.e., forming hierarchically ordered structures over two different length scales).[15i]

Recently, by allowing a toluene solution of an asymmetric comb block copolymer (CBCP) to dry in a "wedge-on-Si" geometry composed of a wedge lens situated on a Si substrate, concentric straight and jagged stripes arranged in a rectangular shape were formed by controlled pinning and depinning cycles of the contact line. Quite interestingly, the formation of straight or jagged stripes strongly depended on the height of the wedge, which influenced the movement speed of the meniscus at the capillary edge.[15e] Subsequent solvent-vapor annealing led to the creation of hierarchically organized structures of CBCP as a result of the synergy between solvent-vapor-assisted unfavorable interfacial-interaction-driven destabilization of the CBCP film from the Si substrate at the microscopic scale and the solvent-vapor-promoted reconstruction of CBCP nanodomains at the nanometer scale. Within the microscopic stripes, the CBCP nanocylinders were aligned either vertically or horizontally to the substrate, depending on the duration of the solvent-vapor treatment.[15e] We note that when a newly synthesized polylactide (PLA) containing bottlebrush block copolymer (PS-PLA BBCP) with a lamellar morphology was used as a nonvolatile solute, hierarchical architectures with nanochannels can be produced by enzymatic degradation of the PLA block in the hierarchically structured BBCP formed by combining the top-down CESA of a toluene solution of PS-PLA BBCP in a "cylinder-on-flat" geometry with the bottom-up spontaneous self-assembly of PS-PLA.[29]

3. Control over Variables

The key to tuning the CESA process to yield a myriad of scalable, complex, and self-organized structures is to precisely control the evaporation process. A number of intrinsic and extrinsic variables should be finely tailored to provide detailed insight into the ordered structure formation from the pinned drying droplets in confined geometries. All of these will modulate the tradeoff between the stable and unstable contact line pinning on which these structures appear to depend.

3.1. Intrinsic Variables

Concentration: Of all the preparation variables, the solution concentration remains one of the most important and intensely studied. In confined geometries, for example, the "curve-on-flat" geometry and the cylindrical tube, the low initial concentration causes less deposition of solutes (i.e., lower height), corresponding to a larger critical contact angle. The pinning time of the contact line is therefore shorter, which in turn leads to a smaller amount of volume loss of solvent during pinning. Thus, a smaller pull of the contact line to next position results (i.e., smaller distance between the neighboring deposits).[15f,j] Different concentrations may also give rise to different and intriguing ordered structures, for example, dots, stripes, and ladders governed by different mechanisms, such as, dewetting, "stick-slip" motion, and fingering instability, respectively.[15a]

Solvent: The choice of solvent is also of key importance in regulating the structure formation. Fast solvent evaporation enhances the convective force through evaporative cooling, thereby forming fingering instabilities, convection cells, fractal branches, and so forth. In contrast, slow solvent evaporation suppresses instabilities, thus yielding highly ordered patterns. It is worth noting that the use of mixed solvents may trigger heterogeneous evaporation of solutions, which promotes the formation of intriguing complex structures in confined geometries.[30] Notably, to facilitate the removal of solvent, a steady flow of gas can be introduced to the confined geometry, thus increasing the evaporation rate.[31]

Composition: A wide spectrum of soft materials with different chemical structures (e.g., amorphous, rubbery, and semicrystalline polymers, as well as conjugated organic molecules and polymers) and inorganic nanomaterials of different types, sizes, and shapes (e.g., nanoparticle, nanorods, tetrapods, disk-like particles, and spherocylinders) can be utilized to self-assemble into a variety of regular isotropic or anisotropic microstructures or nanostructures (e.g., nanowires and nanofibers) influenced by the nature of materials (e.g., strong intermolecular π–π interactions[31]) upon confined evaporation. The ability to process two or more components sequentially[18b] or simultaneously[16a,21e] to form desirable multicomponent structures has been demonstrated on some occasions. When a drying droplet contains a binary mixture of block copolymer/nanoparticle (i.e., polymer A-*b*-polymer B/polymer A (or B)-modified nanoparticles) or a ternary mixture of polymer blend/nanoparticle (i.e., polymer A/polymer B/polymer A (or B)-modified nanoparticles), the synergy of phase separation of polymer blends, co-assembly of surface-functionalized nanoparticles and block copolymers that imparts preferential segregation of nanoparticles within a target block, and the destabilization of polymer mediated by the unfavorable interfacial interaction between the polymer and the substrate during evaporation in confined geometries, may result in appealing complex structures.[30]

Molecular Weight: The variation in molecular weight (M_W) of polymers can lead to a pronounced change in the structure formation. At low molecular weight, the viscosity of the solution front is low and dewetting occurs. Consequently, no contact line is pinned and a liquid-like thin film ruptures, yielding irregular structures.[21c]

3.2. Extrinsic Variables

Surface chemistry: The surface hydrophobicity of confined geometries, which is related to the interfacial interaction between the solute and the substrate, will govern the structure

formation in a predictable way.[30] By capitalizing on the unfavorable interfacial interaction between the solute and the substrate (i.e., possessing a positive Hamaker constant, A), compelling regular structures may be produced through the synergy of CESA of the nonvolatile solute and its destabilization which is effectively mediated by the unfavorable solute/substrate interaction.[10] In addition, the quality of the patterns depends heavily on the nature of the underlying substrate. When the substrate is deliberately chemically modified (e.g., deposited with a functional silane agent), electrostatic interactions or hydrogen bonding between the solute (e.g., positively charged) and the substrate (e.g., negatively charged) can occur during the evaporation process, which may facilitate the adhesion of solutes to the substrate, and thus alters the solute deposition.[32]

Patterned surface: It is not surprising that by patterning the substrate in confined geometries with conventional lithography techniques, for example, creating microscopic or nanoscopic pillars of different shapes, parallel trenches, and so forth on the lower flat substrate, the outward flow that carries the solute to the capillary edge would be markedly modified. The polymer chains, such as DNA and conjugated polymer nanowires, may stretch, align, and immobilize in or around the patterns to form striking self-assembled structures. The combination of topographically patterned surfaces in confined geometries (physical heterogeneity) with chemical modification (chemical heterogeneity) may yield even more unexpected structures.[30]

Geometry: The confined geometry can be tailor-made to craft a rich family of surface patterns with controllable and predictable assembly by CESA. The variation in size, shape, symmetry, and curvature of confined geometries as well as in the separation distance between two surfaces within a confined geometry will inevitably influence the evaporation process and the associated flow field, leading to interesting patterns with different morphologies. These specialized geometries can be further chemically and/or physically modified to afford an even broader range of complex assembled structures.

Temperature: Heating the lower substrate while keeping the upper surface cool would promote the solvent evaporation and impose a temperature gradient, which induces a Marangoni recirculation in the solution.[7f] Drying liquid droplets on the heating substrate has been performed to investigate the dynamics generated by the outgoing matter flow. The Marangoni recirculatory flow driven by the surface-tension gradient could reverse the "coffee ring" phenomenon and produce different deposition patterns.[7f] Notably, the use of patterned heating of the substrate may allow rigorous control over temperature profiles, and thus the manipulation of both the flow and the structure formation.

External field: The application of an additional external field (e.g., magnetic,[33] electric,[28a] and mechanical shear) in conjunction with the solvent evaporative field may be an effective strategy to promote the CESA of polymers and colloids. The external electric or magnetic field could make the deposition process more rapid,[18a] and thus reducing the number of defects in the formed structures, altering the spacing between them (for example, an increase in $\lambda_{C\text{-}C}$ on one side and a decrease of it on the other side when a magnetic field is applied next to the "curve-on-flat" geometry), and potentially achieving improved ordering and orientation of micro- and nanostructures, especially the long-range ordering of nanodomains when block copolymers or block copolymer/nanoparticle mixtures are utilized as nonvolatile solutes.[30] In addition to flow coating as noted in Section 2.2, mechanical perturbations (e.g., vertically pumping or laterally oscillatory shearing the upper surface in confined geometries) can be introduced during the CESA processes to impart or perturb the deposition patterns by modifying the flow symmetrically (i.e., pumping) or unidirectionally (i.e., oscillatory shearing) at the proper frequency and amplitude. Moreover, when DNA is used, air blowing may be applied in the confined geometry to expedite the evaporation process and align DNA to give 1D DNA nanofibers that may exceed several hundred micrometers in length (i.e., molecular combing of DNA[34]).

4. Summary and Outlook

This Review highlights simple, cheap yet controllable and robust preparative strategies based on the CESA of confined solutions to assemble various soft and hard materials, including polymers, biomolecules, nanoparticles, into spatially ordered structures with engineered properties and functionality over large surface areas. The confined geometry imparts a unique environment for exquisite control over the flow within the drying droplet, which in turn promotes the formation of highly regular complex structures. The scope of potential applications for such structures is vast, encompassing combinatorial chemistry, inkjet printing, electronics, optical coatings with selective or enhanced transmittance, optical materials, photonics, optoelectronics, energy conversion and storage, microfluidic devices, magnetic materials, information processing and data storage devices, multifunctional materials and devices, nanotechnology, sensors, DNA/RNA microarrays, gene mapping of DNA, high-throughput drug discovery, and biotechnology.[30] Future work in this extraordinarily rich field will likely include the following directions: theory and simulations on deposition patterns, three dimensional assemblies, hierarchically ordered structures, and in-situ visualization of structural anisotropy and assembly/crystallization process.

The ability to predict the length scales of periodicity, height, and width as a function of the wealth of variables noted in Section 3, and then compare them with experimental observations, is the key to understanding the mechanisms of structure formation by CESA in confined geometries.[30] Clearly, the rich deposition patterns resulting from controlled evaporation require detailed theoretical studies and computer simulations to provide a basis for fully understanding the assembly process and identifying assembly pathways to produce controllable and consistent depositions in confined geometries. This remains challenging as the determination of the evaporation profile with these nonconventional boundary geometries, rather than a simple geometry (i.e., spherical cap in a sessile droplet) is one of the primary obstacles for rigorously solving the deposition problem.

It is noteworthy that 1D and 2D ordered structures can be readily achieved by current state-of-art CESA approaches. In contrast, effective methods to prepare 3D structures are rather few and limited in scope. In principle, it is highly desirable to create 3D structures for many potential applications, such as photonic crystals, electronics, micro-electromechanical systems (MEMS). Innovative approaches based on extremely simple evaporative assembly to rationally craft 3D structured materials and devices should be developed. One route that may lead to 3D assembly and ordering is to exploit patterned substrates of suitable dimensions and aspect ratios,[35] that are either simply physically or both chemically and physically patterned, to guide the transport of solutes to fill the patterns or deposit in the vicinity of the patterns.[30] Furthermore, 3D structures may also be realized by performing staged or sequential assembly processes in the confined geometry.

Hierarchical structures are common in both nature and technology. The combination of CESA in confined geometries with smaller-scale molecular self-assembly (e.g., block copolymers) leads to hierarchically ordered structures with specific synergetic properties that would offer new opportunities for many applications in the areas of electronics, optics, and energy storage. We note the formation of the block-copolymer-based hierarchical ordered structures often requires subsequent thermal annealing[15b,24] or selective solvent-vapor annealing[15e,i] to achieve the ordering and orientation of nanodomains within the microstructure formed by CESA. In this context, it is of great interest to explore powerful and efficient methods to develop hierarchically ordered functional structures with precisely controlled dimension, function, and topology in one-step, eliminating the annealing treatments. This advance is of particular importance when block copolymer/nanoparticle mixtures are used[36] as tremendous challenges remain in the simultaneous controllable incorporation of nanoparticles within the target block and the ordering and orientation of block copolymers within the CESA-induced microscopic structures, to provide functions and forms at multiple scales and locations. It is worth noting that ordered hierarchical assemblies composed of nanocrystals (e.g., quantum dots, QDs) as building blocks have been prepared,[18b] however the QDs within submicron-to-micron wide patterns are often randomly arranged or aggregated. Recent advances in the synthesis of nanocrystals have allowed the growth of a variety of nanocrystals of different sizes, shapes, and functionality. A possible route to assembling nanocrystals into ordered arrays (i.e., superlattice[37]) within structured patterns by CESA (i.e., forming hierarchically assembled nanocrystals over multiple length scales) will be to expedite the controlled evaporation process (i.e., faster solvent evaporation rate) by tailoring the variables discussed in Section 3. Future development of hierarchically ordered structures by CESA to give greater functionality and complexity will probably involve the concurrent multicomponent self-assembly by exploiting the shape of solutes, intermolecular interactions, induced conformation changes of solutes, tailored solute/substrate interactions, phase segregation, external fields, and so forth.

The liquid evaporates from the droplet edge in confined geometries should largely affect the flow of fluid inside the droplet. Thus, the determination of flow profiles in the droplet will help understand the solute transport and/or redistribution under different experimental conditions,[3] such flow profiles could be determined by monitoring fluorescent solutes using particle image velocimetry. To map the flow profiles inside an evaporating droplet containing polymer chains that may crystallize or self-assemble into nanostructures during the course of solvent evaporation, it is vital to utilize or develop novel optical characterization techniques that can offer reliable and appropriate measurement.[30] For example, fluorescence dynamics images the trajectory of polymer chains, in-situ angular dependent polarized Raman spectroscopy monitors the Raman shift as a function of time to provide information on evolution of the chain alignment,[38] and rapid scan time-resolved infrared spectroscopy studies the in-situ crystallization induced by evaporation.[39] Moreover, it would be invaluable to exploit state-of-art spectroscopic techniques to probe the simultaneous occurrence of phase segregation, assembly, and crystallization in the proximity of the moving three-phase contact lines in real time, which may remain as an active area of exploration.

We gratefully acknowledge support from the National Science Foundation (NSF CBET-0844084 and NSF CMMI-0968656)

Received: June 28, 2011
Published online: December 23, 2011

[1] a) R. D. Deegan, O. Bakajin, T. F. Dupont, G. Huber, S. R. Nagel, T. A. Witten, *Nature* **1997**, *389*, 827–829; b) R. D. Deegan, O. Bakajin, T. F. Dupont, G. Huber, S. R. Nagel, T. A. Witten, *Phys. Rev. E* **2000**, *62*, 756–765; c) E. Rabani, D. R. Reichman, P. L. Geissler, L. E. Brus, *Nature* **2003**, *426*, 271–274; d) B. P. Khanal, E. R. Zubarev, *Angew. Chem.* **2007**, *119*, 2245–2248; *Angew. Chem. Int. Ed.* **2007**, *46*, 2195–2198.

[2] a) E. Adachi, A. S. Dimitrov, K. Nagayama, *Langmuir* **1995**, *11*, 1057–1060; b) L. Shmuylovich, A. Q. Shen, H. A. Stone, *Langmuir* **2002**, *18*, 3441–3445.

[3] B. J. Fischer, *Langmuir* **2002**, *18*, 60–67.

[4] Y. O. Popov, *Phys. Rev. E* **2005**, *71*, 036313.

[5] K. Ozawa, E. Nishitani, M. Doi, *Jpn. J. Appl. Phys.* **2005**, *44*, 4229–4234.

[6] a) M. Nonomura, R. Kobayashi, Y. Nishiura, M. Shimomura, *J. Phys. Soc. Jpn.* **2003**, *72*, 2468–2471; b) L. Frastia, A. J. Archer, U. Thiele, *Phys. Rev. Lett.* **2011**, *106*, 077801.

[7] a) S. Q. Xu, E. Kumacheva, *J. Am. Chem. Soc.* **2002**, *124*, 1142–1143; b) Z. Mitov, E. Kumacheva, *Phys. Rev. Lett.* **1998**, *81*, 3427–3430; c) V. X. Nguyen, K. J. Stebe, *Phys. Rev. Lett.* **2002**, *88*, 164501; d) A. V. Getling, O. Brausch, *Phys. Rev. E* **2003**, *67*, 046313; e) I. Tuval, L. Cisneros, C. Dombrowski, C. W. Wolgemuth, J. Kessler, R. E. Goldstein, *Proc. Natl. Acad. Sci. USA* **2005**, *102*, 2277–2282; f) H. Hu, R. G. Larson, *J. Phys. Chem. B* **2006**, *110*, 7090–7094; g) H. Hu, R. G. Larson, *Langmuir* **2005**, *21*, 3963–3971.

[8] R. D. Deegan, *Phys. Rev. E* **2000**, *61*, 475–485.

[9] M. Maillard, L. Motte, M. P. Pileni, *Adv. Mater.* **2001**, *13*, 200–204.

[10] S. W. Hong, J. F. Xia, Z. Q. Lin, *Adv. Mater.* **2007**, *19*, 1413–1417.

[11] E. Pauliac-Vaujour, A. Stannard, C. P. Martin, M. O. Blunt, I. Notingher, P. J. Moriarty, I. Vancea, U. Thiele, *Phys. Rev. Lett.* **2008**, *100*, 176102.

[12] a) M. Gleiche, L. F. Chi, H. Fuchs, *Nature* **2000**, *403*, 173–175; b) X. Chen, A. L. Rogach, D. V. Talapin, H. Fuchs, L. F. Chi, *J. Am. Chem. Soc.* **2006**, *128*, 9592–9593.

[13] J. Huang, F. Kim, A. R. Tao, S. Connor, P. D. Yang, *Nat. Mater.* **2005**, *4*, 896–900.

[14] B. G. Prevo, O. D. Velev, *Langmuir* **2004**, *20*, 2099–2107.

[15] a) H. Yabu, M. Shimomura, *Adv. Funct. Mater.* **2005**, *15*, 575–581; b) B. H. Kim, D. O. Shin, S.-J. Jeong, C. M. Koo, S. C. Jeon, W. J. Hwang, S. Lee, M. G. Lee, S. O. Kim, *Adv. Mater.* **2008**, *20*, 2303–2307; c) Z. Q. Lin, S. Granick, *J. Am. Chem. Soc.* **2005**, *127*, 2816–2817; d) S. W. Hong, J. Xu, J. F. Xia, Z. Q. Lin, F. Qiu, Y. L. Yang, *Chem. Mater.* **2005**, *17*, 6223–6226; e) M. Byun, N. B. Bowden, Z. Lin, *Nano Lett.* **2010**, *10*, 3111–3117; f) J. Xu, J. F. Xia, S. W. Hong, Z. Q. Lin, F. Qiu, Y. L. Yang, *Phys. Rev. Lett.* **2006**, *96*, 066104; g) J. Xu, J. F. Xia, Z. Q. Lin, *Angew. Chem.* **2007**, *119*, 1892–1895; *Angew. Chem. Int. Ed.* **2007**, *46*, 1860–1863; h) S. W. Hong, M. Byun, Z. Q. Lin, *Angew. Chem.* **2009**, *121*, 520–524; *Angew. Chem. Int. Ed.* **2009**, *48*, 512–516; i) S. W. Hong, J. Wang, Z. Q. Lin, *Angew. Chem.* **2009**, *121*, 8506–8510; *Angew. Chem. Int. Ed.* **2009**, *48*, 8356–8360; j) M. Abkarian, J. Nunes, H. A. Stone, *J. Am. Chem. Soc.* **2004**, *126*, 5978–5979; k) Y. Lin, E. Balizan, L. A. Lee, Z. Niu, Q. Wang, *Angew. Chem.* **2010**, *122*, 880–884; *Angew. Chem. Int. Ed.* **2010**, *49*, 868–872.

[16] a) D. J. Harris, H. Hu, J. C. Conrad, J. A. Lewis, *Phys. Rev. Lett.* **2007**, *98*, 148301; b) D. J. Harris, J. A. Lewis, *Langmuir* **2008**, *24*, 3681–3685.

[17] a) L. Jiang, H. Dong, W. Hu, *Soft Matter* **2011**, *7*, 1615–1630; b) U. H. F. Bunz, *Adv. Mater.* **2006**, *18*, 973–989.

[18] a) J. Kleinert, S. Kim, O. D. Velev, *Langmuir* **2010**, *26*, 10380–10385; b) H. S. Kim, C. H. Lee, P. K. Sudeep, T. Emrick, A. J. Crosby, *Adv. Mater.* **2010**, *22*, 4600–4604.

[19] Y. Lin, Z. Su, E. Balizan, Z. Niu, Q. Wang, *Langmuir* **2010**, *26*, 12803–12809.

[20] D. J. Harris, J. C. Conrad, J. A. Lewis, *Philos. Trans. R. Soc. London Ser. A* **2009**, *367*, 5157–5165.

[21] a) S. W. Hong, S. Giri, V. S. Y. Lin, Z. Q. Lin, *Chem. Mater.* **2006**, *18*, 5164–5166; b) S. W. Hong, J. Xu, Z. Q. Lin, *Nano Lett.* **2006**, *6*, 2949–2954; c) S. W. Hong, J. F. Xia, M. Byun, Q. Z. Zou, Z. Q. Lin, *Macromolecules* **2007**, *40*, 2831–2836; d) S. W. Hong, W. Jeong, H. Ko, M. R. Kessler, V. V. Tsukruk, Z. Q. Lin, *Adv. Funct. Mater.* **2008**, *18*, 2114–2122; e) M. Byun, S. W. Hong, F. Qiu, Q. Z. Zou, Z. Q. Lin, *Macromolecules* **2008**, *41*, 9312–9317; f) M. Byun, S. W. Hong, L. Zhu, Z. Lin, *Langmuir* **2008**, *24*, 3525–3531; g) M. Byun, R. L. Laskowski, M. He, F. Qiu, M. Jeffries-El, Z. Q. Lin, *Soft Matter* **2009**, *5*, 1583–1586; h) M. Byun, J. Wang, Z. Q. Lin, *J. Phys. Condens. Matter* **2009**, *21*, 264014; i) M. Byun, W. Han, F. Qiu, N. B. Bowden, Z. Lin, *Small* **2010**, *6*, 2250–2255; j) W. Han, M. Byun, Z. Lin, *J. Mater. Chem.* **2011**, *21*, 16968–16972.

[22] a) V. L. Colvin, M. C. Schlamp, A. P. Alivisatos, *Nature* **1994**, *370*, 354–357; b) A. P. Alivisatos, *Abstr. Pap. Am. Chem. Soc.* **2004**, *227*, 1240; c) I. L. Medintz, H. T. Uyeda, E. R. Goldman, H. Mattoussi, *Nat. Mater.* **2005**, *4*, 435–446.

[23] a) J. Xu, J. Wang, M. Mitchell, P. Mukherjee, M. Jeffries-EL, J. W. Petrich, Z. Q. Lin, *J. Am. Chem. Soc.* **2007**, *129*, 12828–12833; b) J. Xu, J. F. Xia, J. Wang, J. Shinar, Z. Q. Lin, *Appl. Phys. Lett.* **2006**, *89*, 133110; c) D. Zimnitsky, C. Jiang, J. Xu, Z. Q. Lin, V. V. Tsukruk, *Langmuir* **2007**, *23*, 4509–4515; d) D. Zimnitsky, C. Jiang, J. Xu, Z. Q. Lin, L. Zhang, V. V. Tsukruk, *Langmuir* **2007**, *23*, 10176–10183; e) J. Wang, J. Xu, M. D. Goodman, Y. Chen, M. Cai, J. Shinar, Z. Q. Lin, *J. Mater. Chem.* **2008**, *18*, 3270–3274; f) Z. Q. Lin, *Chem. Eur. J.* **2008**, *14*, 6294–6301; g) M. D. Goodman, J. Xu, J. Wang, Z. Q. Lin, *Chem. Mater.* **2009**, *21*, 934–938.

[24] B. H. Kim, H. M. Lee, J. H. Lee, S. W. Son, S. J. Jeong, S. Lee, D. I. Lee, S. U. Kwak, H. Jeong, H. Shin, J. B. Yoon, O. D. Lavrentovich, S. O. Kim, *Adv. Funct. Mater.* **2009**, *19*, 2584–2591.

[25] a) Y.-H. Lin, C. Y. Jiang, J. Xu, Z. Q. Lin, V. V. Tsukruk, *Adv. Mater.* **2007**, *19*, 3827–3832; b) L. Zhao, X. Pang, R. Adhikary, J. Petrich, M. Jeffries-EL, Z. Lin, *Adv. Mater.* **2011**, *23*, 2844–2849; c) L. Zhao, X. Pang, R. Adhikary, J. Petrich, Z. Lin, *Angew. Chem.* **2011**, *123*, 4044–4048; *Angew. Chem. Int. Ed.* **2011**, *50*, 3958–3962.

[26] a) M. He, L. Zhao, J. Wang, W. Han, Y. L. Yang, F. Qiu, Z. Q. Lin, *ACS Nano* **2010**, *4*, 3241–3247; b) M. He, W. Han, J. Ge, Y. L. Yang, F. Qiu, Z. Lin, *Energy Environ. Sci.* **2011**, *4*, 2894-2902; c) M. He, W. Han, J. Ge, W. Yu, Y. L. Yang, F. Qiu, Z. Lin, *Nanoscale* **2011**, *3*, 3159–3163.

[27] T. Y. Kim, S. W. Kwon, S. J. Park, D. H. Yoon, K. S. Suh, W. S. Yang, *Adv. Mater.* **2011**, *23*, 2734–2738.

[28] a) T. Thurn-Albrecht, J. Schotter, C. A. Kastle, N. Emley, T. Shibauchi, L. Krusin-Elbaum, K. Guarini, C. T. Black, M. T. Tuominen, T. P. Russell, *Science* **2000**, *290*, 2126–2129; b) J. Y. Cheng, C. A. Ross, H. I. Smith, E. L. Thomas, *Adv. Mater.* **2006**, *18*, 2505–2521; c) S. Ouk Kim, H. H. Solak, M. P. Stoykovich, N. J. Ferrier, J. J. de Pablo, P. F. Nealey, *Nature* **2003**, *424*, 411–414; d) C. J. Hawker, T. P. Russell, *MRS Bull.* **2005**, *30*, 952–966.

[29] W. Han, M. Byun, L. Zhao, J. Rzayev, Z. Lin, *J. Mater. Chem.* **2011**, 21, 14248–14253.

[30] Z. Lin, *J. Polym. Sci. Part B* **2010**, *48*, 2552–2557.

[31] Z. Wang, R. Bao, X. Zhang, X. Ou, C.-S. Lee, J. C. Chang, X. Zhang, *Angew. Chem.* **2011**, *123*, 2863–2867; *Angew. Chem. Int. Ed.* **2011**, *50*, 2811–2815.

[32] a) J. Chen, W. Liao, X. Chen, T. Yang, S. E. Wark, D. Son, J. D. Batteas, P. S. Cremer, *ACS Nano* **2009**, *3*, 173–180; b) M. A. Ray, H. Kim, L. Jia, *Langmuir* **2005**, *21*, 4786–4789.

[33] S. L. Tripp, S. V. Pusztay, A. E. Ribbe, A. Wei, *J. Am. Chem. Soc.* **2002**, *124*, 7914–7915.

[34] X. Michalet, R. Ekong, F. Fougerousse, S. Rousseaux, C. Schurra, N. Hornigold, M. van Slegtenhorst, J. Wolfe, S. Povey, J. S. Beckmann, A. Bensimon, *Science* **1997**, *277*, 1518–1523.

[35] S. Choi, S. Stassi, A. P. Pisano, T. I. Zohd, *Langmuir* **2010**, *24*.

[36] Y. Lin, A. Boker, J. He, K. Sill, H. Xiang, C. Abetz, X. Li, J. Wang, T. Emrick, S. Long, Q. Wang, A. Balazs, T. P. Russell, *Nature* **2005**, *434*, 55–59.

[37] A. Dong, J. Chen, S. J. Oh, W. K. Koh, F. Xiu, X. Ye, D. K. Ko, K. L. Wang, C. R. Kagan, C. B. Murray, *Nano Lett.* **2011**, *11*, 841–846.

[38] M. S. Park, A. Aiyar, J. O. Park, E. Reichmanis, M. Srinivasarao, *J. Am. Chem. Soc.* **2011**, *133*, 7244–7247.

[39] P. Innocenzi, L. Malfatti, M. Piccinini, A. Marcelli, *J. Phys. Chem. A* **2010**, *114*, 304–308.